# Development of Sprayable Engineered Cementitious Composites (SECC) for Tunnel Lining Applications

S.N. Goh, K.L. Lo, Ivan H.H. Chan & Roy K.C. Hung
*Geotechnical Engineering Office, Civil Engineering and Development Department*

T. Wang & H. Wu
*Formerly Department of Civil and Environmental Engineering,*
*The Hong Kong University of Science and Technology*

Christopher K.Y. Leung
*Department of Civil and Environmental Engineering, The Hong Kong University of Science and Technology*

Victor C. Li
*Department of Civil and Environmental Engineering, University of Michigan*

doi: https://doi.org/10.21467/proceedings.8.2.3

## ABSTRACT

Engineered cementitious composites (ECC) are characterised by tensile strain-hardening, multi-cracking response and self-healing capacity, delivering exceptional ductility, durability and sustainability for civil infrastructure. A study was launched in 2021 by the Geotechnical Engineering Office (CEDD) to develop a sprayable ECC (SECC) for tunnel lining in mixed ground and hard rock conditions. This paper outlines the theoretical basis, mix design, and mechanical performance of SECC, with emphasis on findings from the scale-up production and site spray trials at the Joint Cavern Development, Anderson Road Quarry Site, in Phase II. Results confirm SECC's feasibility and highlight key process-control considerations, with recommendations for optimising mixing and spraying methods to enhance its suitability for tunnel lining in Hong Kong. As ECC's ductile, strain-hardening behaviour extends beyond the linear-elastic–perfectly-plastic framework codified in local practice, its full utilisation will depend on progressive refinements in structural design methodology, ensuring future frameworks evolve to capture its potential.

## 1 INTRODUCTION

### *1.1 Background of the study*

Engineered Cementitious Composites (ECC) refers to a class of ultra-ductile fibre-reinforced cementitious composites characterised by tensile strain-hardening, multi-cracking and self-healing properties (Li & Leung, 1992). Unlike common fibre-reinforced concrete (FRC), ECC is designed using fundamental principles of fracture mechanics and micromechanics to analyse and utilise the fibre bridging property, thereby controlling the formation of steady-state flat microcracks across the matrix (Li, 2003). Meticulous calibration of the fibre-matrix-interface characteristics is often required to design and manufacture an ECC mix (Li, 2003). These engineered attributes have enabled widespread applications of ECC in infrastructure projects across the United States, Japan, and the Chinese Mainland, as well-documented by (Li, 2019), demonstrating its contributions to more resilient, durable and sustainable urban development.

In sprayed concrete applications for tunnel linings, ECC would be applied as a thinner overlay on the rock substrate when comparing to traditional cast-in-situ concrete structures. Depending on the ground conditions, the lining may need to withstand bending arising from earth loads and local instabilities (e.g. rock wedges, fault zones, etc.), inducing primarily flexural tensile stresses. This demands tailored mix formulations to ensure sprayability while maintaining structural integrity under bending. Self-controlled, tight crack width of ECC is advantageous for water impermeability in underground facilities. Further, dimensional stability and vibration resistance are necessary for the successful deployment of ECC in tunnel lining applications.



© 2026 Copyright held by the author(s). Published by AIJR Publisher in " Proceedings of The HKIE Geotechnical Division 46th Annual Seminar 2026: Bridging Theory and Practice in Geotechnical Engineering" (GDAS2026). Organized by the Geotechnical Division, The Hong Kong Institution of Engineers, Hong Kong on May 12, 2026.

Proceedings DOI: 10.21467/proceedings.8.2; Series: AIJR Proceedings; ISSN: 2582-3922; ISBN: 978-81-688301-1-0

### *1.2 Objectives of the study and structure of this paper*

Motivated by the limited adoption of ECC in Hong Kong—primarily in a housing project as repair mortar (see (Li, 2019), Chapter 9, Section 9.2.3.1)—and the unique challenges of tunnel and cavern environments, the Geotechnical Engineering Office (GEO) of the Civil Engineering and Development Department (CEDD) initiated a developmental project on Sprayable Engineered Cementitious Composites (SECC) that preserve core ECC properties while meeting tunnelling-specific demands. This study has two primary objectives: (i) to conceptualise, design and produce suitable SECC mixes using locally available materials; and (ii) to evaluate end-to-end logistics from scale-up production at a concrete batching plant to on-site spraying. This paper presents key findings addressing both objectives, emphasising the benefits of SECC linings, while discussing study limitations, potential challenges and practical recommendations for future large-scale, routine applications.

## 2 DESIGN OF SECC MIXES

### *2.1 Mix conceptualisation and formulation*

This study adopted a performance-oriented, iterative approach to SECC design for tunnel linings, targeting balanced sprayability, early-age build-up, mechanical performance, self-healing, and self-stressing, building on knowledge gained from prior research on self-stressing ECC (Zhu et al, 2021). Self-stressing is induced by the controlled expansion of the ECC mix (during curing) restrained by a structural boundary or a rock substrate. Baseline ECC formulations were first developed in the laboratory to achieve fresh-state deformability, setting, and tensile strain-hardening. Key parameters—calcium sulfoaluminate (CSA)/binder ratio, water-to-binder ratio, sand content, and superplasticizer dosage—were systematically adjusted to optimise deformability, penetration resistance, and strength development, capitalising on CSA's high early-age reactivity. OPC served as the primary binder, with CSA added for early hydration and self-stressing control, while ground granulated blast-furnace slag (GGBS) or pulverized fly ash (PFA) and mesh 80–120 quartz sand were incorporated to enhance durability, sustainability and cost-effectiveness. Addition of polyvinyl alcohol (PVA) fibres (Kuraray, Japan; properties in Table 1) ensured composite tensile ductility, fibre dispersion, and tight crack-width control.

Selected mixes were then subjected to laboratory trials, with further modifications including expansion agents, anhydrite, shrinkage-reducing agents, viscosity-modifying admixtures, and retarders to improve volume stability, crack control, build-up thickness, and spraying operability under practical conditions.

For laboratory mixing, all mixes were prepared in a Hobart mixer following a standardised procedure: (i) dry mixing of solid materials for 5 minutes; (ii) addition of water and mixing for 2 minutes; (iii) fibre incorporation and mixing for 3 minutes; and (iv) addition of superplasticizer and mixing for 2 minutes. For chemical admixtures, other than super-plasticisers, hydroxypropyl methylcellulose (HPMC; Alfa Aesar, viscosity 7500–14,000 mPa·s) was added at 0.1% to 0.3% of binder for viscosity modification.

Table 1: Nominal properties of polyvinyl alcohol (PVA) fibre

| Length (mm) | Diameter (μm) | Aspect ratio | Elastic Modulus (GPa) | Fibre strength (MPa) | Fibre density (g/cm3) |
|---|---|---|---|---|---|
| 12 | 39 | 308 | 40 | 1600 | 1.30 |

The final SECC mixes–one with GGBS and another with PFA–are summarised in Table 2 below. The selected mixes exhibited satisfactory sprayability, controlled stiffening suitable for build-up, 28-day mean compressive strength in the approximate range of 45 MPa to 55 MPa, tensile strain-hardening performance with strain capacities exceeding 1.5-2.0%, and tight crack-width control conducive to self-healing.

Table 2: Mix proportions of the final selected SECC (mass ratio, PVA fibre vol. ratio 0.02)

| Mix ID | OPC | CSA | SCM* | Water | Sand | HPMC | SP |
|---|---|---|---|---|---|---|---|
| GGBS-ECC | 0.65 | 0.35 | 1.0 | 0.90 | 0.72 | 0.003 | 0.002 |
| PFA-ECC | 0.70 | 0.30 | 2.0 | 0.80 | 0.80 | 0.001 | 0.002 |

* SCM means supplementary cementitious materials, referring to either GGBS or PFA.

Proceedings DOI: 10.21467/proceedings.8.2
ISBN: 978-81-688301-1-0

Series: AIJR Proceedings
ISSN: 2582-3922

### *2.2 Functional mechanisms of SECC for tunnel lining applications*

In principle, SECC shall maintain structural integrity subject to impact loading, while simultaneously limiting crack-induced durability degradation (Khandelwal & Singh, 2009, Koo et al., 2013, Ding et al., 2020). Self-healing and self-stressing behaviours are thus introduced as complementary functional mechanisms, targeting long-term durability and early-age crack control, respectively. These mechanisms are discussed below to elucidate their engineering implications in tunnel lining applications.

#### *2.2.1 Self-healing mechanism*

During tunnelling construction, impact loading from blasting or mechanical excavation, together with early-stage tunnel convergence, may induce cracking in lining materials, accelerating water and chemical ingress and compromising durability. While residual mechanical capacity is essential for structural safety, the ability to autonomously seal cracks after damage is equally critical for long-term performance. Impact tests were performed using pendulum loading (drop heights 0.92 m to 1.28 m) and Split Hopkinson Pressure Bar (SHPB) (impact speeds from 2 m/s to 6 m/s) calibrated through numerical modelling of tunnel blasting. Owing to ECC's strain-hardening behaviour and multiple microcracking, most induced cracks remained narrow (in μm) and exhibited satisfactory residual performance in compression, tension, bending and bonding. Crack-width evolution was subsequently monitored under continuous moisture exposure and wet–dry cycling (two days per cycle, with wet curing as the initial step).

Figure 1(a) below presents the evolution of average crack width with curing age under different exposure conditions. Under continuous moisture exposure, crack widths remain nearly unchanged even after prolonged curing, indicating negligible self-healing. In contrast, specimens subjected to wet – dry cycling exhibit pronounced crack closure, with fine cracks (initial widths $\leqslant$ ~127 μm) being fully sealed after several cycles. Representative visual observations of crack evolution are shown in Figure 1(b) to (d), which illustrates the absence of visible healing under moisture exposure and effective crack sealing achieved under wet–dry cycling.

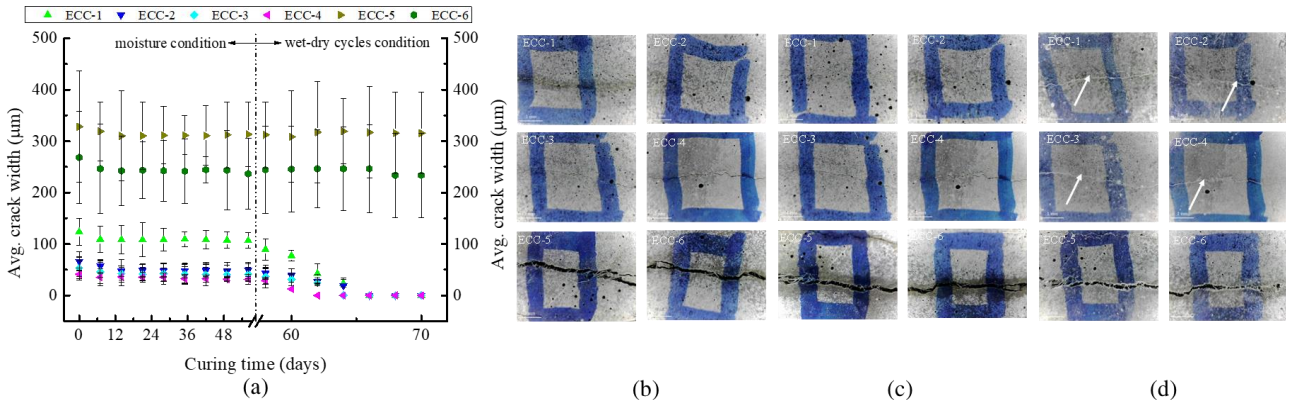



Figure 1: (a) Variations of average crack width with curing ages; and self-healing phenomenon of cracked ECC-specimens (b) 7-day in moisture exposure, (c) 56 days in moisture exposure, and (d) 7 cycles in wet-dry exposure

The underlying self-healing mechanisms were further examined through microstructural characterisation. Scanning electron microscopy (SEM) images of healed cracks (Figure 2(a)) revealed that healing products densely fill the crack surfaces and progressively bridge opposing crack faces. Energy-dispersive X-ray (EDX) analysis of the healing products (Figure 2(b)) indicated that Ca, Si, C, and O are the dominant elements, confirming that the primary healing phases consist of calcium silicate hydrate (C–S–H) and calcium carbonate. These products originate from continued hydration of unreacted cementitious materials and carbonation-induced precipitation during wet–dry cycling.

The concentration of healing products near the crack surface explains why surface crack closure is dominant, while deeper crack regions remain largely unhealed. Nevertheless, sealing of surface-connected cracks is sufficient to significantly reduce permeability and limit water and ion ingress, thereby enhancing durability. The high ductility, multiple micro-cracking behaviour, and tight crack width control of ECC strongly facilitate this

autogenous self-healing process, as narrower cracks require fewer healing products and enable more efficient crack closure (Ghosh, 2009; Van Tittelboom & De Belie, 2013, Yang et al., 2011).

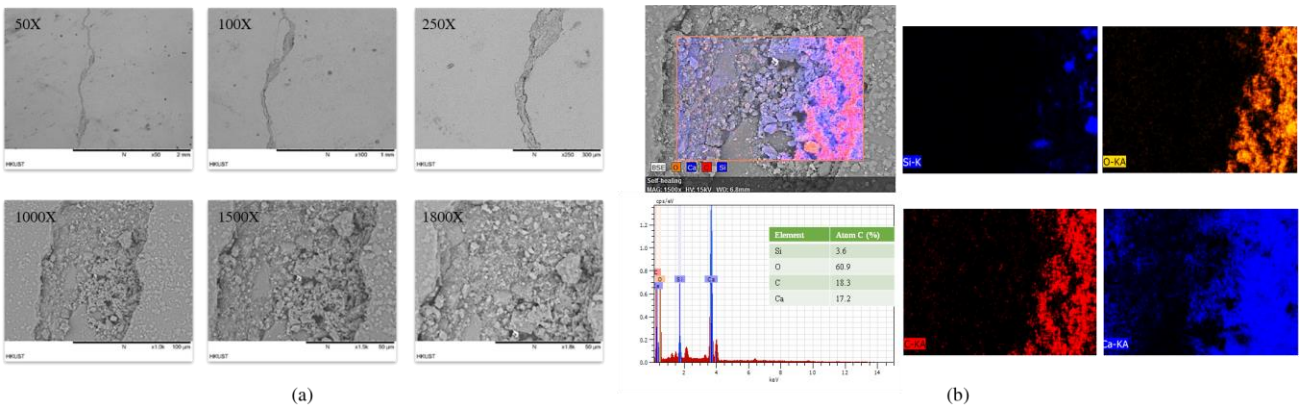



Figure 2: (a) SEM images of self-healed crack (magnification from 50 to 1800 times); and (b) EDX analysis on the self-healing materials

### *2.2.2 Self-stressing mechanism and volume stability control*

In addition to self-healing, self-stressing behaviour was introduced to mitigate shrinkage-induced cracking and improve early-age structural integrity of SECC. The design of self-stressing SECC followed established approaches using CSA-based expansive components (Zhu et al., 2021). Figure 3 illustrates the typical free expansion behaviour of self-stressing ECC mixes with varying CSA contents. Increasing CSA content led to enhanced early-age expansion, with most expansion occurring within the first few days.

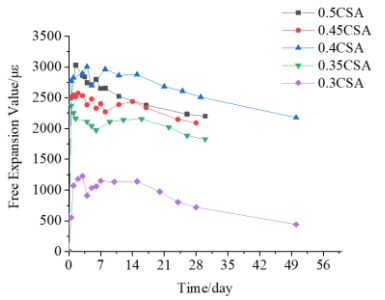



Figure 3: Free expansion/shrinkage measurement of ECC mixes

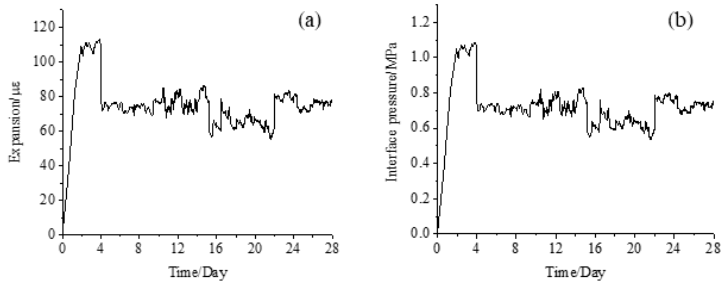



Figure 4: (a) Expansion and (b) interface pressure in the steel ring tests

To evaluate the effectiveness of expansion under restrained conditions, ECC was cast inside a steel ring. Figure 4 above shows the measured expansion of the steel ring and the corresponding interface pressure generated by the expansive ECC. The results confirmed that the early-age expansion translated into beneficial compressive pressure at the ECC–steel interface, indicating improved contact and load transfer under restraint. This phenomenon effectively serves as a self-induced mechanical coupling between the sprayed ECC layer and the surrounding restraint. Importantly, the incorporation of expansive components did not compromise the strain-hardening behaviour of ECC, demonstrating that self-stressing and tensile ductility could be achieved simultaneously.

### *2.3 Mix refinement for sprayability and build-up capacity*

Beyond functional mechanisms, practical application of SECC requires adequate sprayability and build-up capacity during construction. Figure 5 compares the maximum achievable build-up thickness before and after mix refinement. The optimised SECC exhibits a one-time build-up thickness exceeding 60 mm, compared with

Proceedings DOI: 10.21467/proceedings.8.2
ISBN: 978-81-688301-1-0

Series: AIJR Proceedings
ISSN: 2582-3922

approximately 25 mm for the unmodified mix. According to Qian et al. (2025), tunnel lining materials should achieve a minimum one-time build-up thickness of 40–50 mm to ensure construction efficiency and structural integrity. The refined SECC mixes therefore satisfy practical construction requirements and are suitable materials for spray-applied tunnel lining applications. Sprayability and build-up capacity were further assessed in the scale-up production trial and site spray trial as discussed in Section 3 and Section 4 respectively.



Figure 5: Improvement of sprayability and build-up capacity through laboratory trials

## 3 SCALE-UP PRODUCTION AT A CONCRETE BATCHING PLANT

To test and verify the quality and consistency of the two SECC mixes in a large-scale production, two scale-up production trials were conducted at Shunde Lunjiao Quon Hing Construction Material Company (Figure 6(a)).

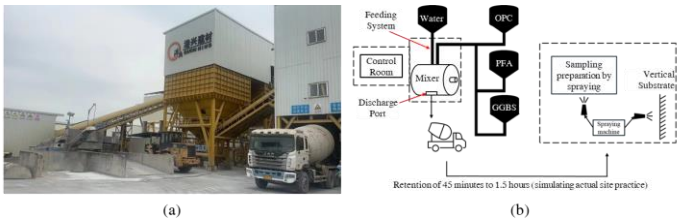



Figure 6: (a) Quon Hing concrete batching plant in Foshan; and (b) schematics of scale-up production

Table 3: Mix proportions (mass ratio, PVA fibre vol. ratio 0.02), each in a volume of 1.2 $m^3$

| Mix ID | OPC | CSA | SCM | Water | Sand | HPMC | SP |
|---|---|---|---|---|---|---|---|
| GGBS-ECC | 0.65 | 0.35 | 1.00 | 0.90 | 0.72 | 0.003 | 0.002 |
| PFA-ECC | 0.70 | 0.30 | 1.20 | 0.80 | 0.80 | 0.001 | 0.002 |

The scale-up production consists of two stages: (i) plant mixing of two SECC mixes developed at HKUST Concrete Laboratory; and (ii) an investigation of the mechanical and applicational properties of the SECC mixes produced. The previous mix design and constituent material proportions in the SECC mixes were further optimised and calibrated based on laboratory performance. All materials were sourced from Foshan, the Chinese Mainland, and supplied by Quon Hing. These constituent materials demonstrated equivalent physical and chemical properties to those employed in the laboratory mix design stage (Section 2) and the site trial stage (Section 4).

The mix compositions are summarised in Table 3 above. For chemical admixtures, a shrinkage-reducing agent (SRA from Sobute, shrinkage reduction rate 30%) and an expansion agent (EA from TUNIU), which mainly consist of CSA and anhydrite (from LeiXin, with $CaSO_4$ content of over 95% and water content of less than 0.5%), were employed.

The schematic diagram of the scale-up production is shown in Figure 6(b) above. The OPC, GGBS, and PFA are in stock at the concrete batching plant and can be fed into the mixer through the feeding system. The other dry materials including sand, PVA fibre and various additives are manually added into the mixer. The moulds for sample preparation through spraying method are placed in an orderly manner on site (Figure 7(a)). The vertical substrates used to simulate practical spraying work are shown in Figure 7(b).



(a) (b)

Figure 7: (a) Moulds for test specimens and (b) vertical wall substrates

### 3.2 Flexure and energy absorption (toughness) performance

Flexure tests were performed in accordance with ASTM C1609. A Shanghai SUNS UTM2502 Electromechanical Universal Testing Machine was used for this test. The load-central deflection curves for the two SECC mixes are shown in Figure 8. Multiple cracks were observed across the test specimens as shown in Figure 11(a) below.

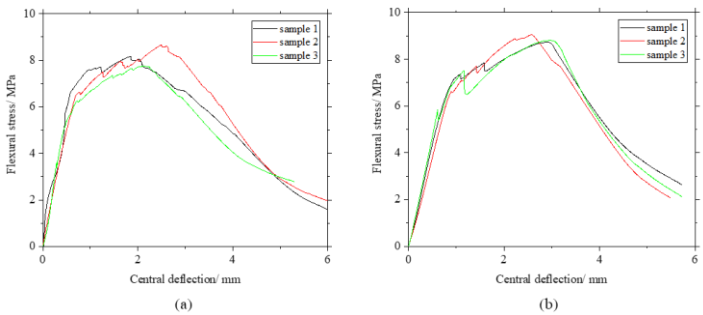



Figure 8: Flexural stress versus central deflection curves for (a) GGBS-ECC and (b) PFA-ECC beams

Table 4 shows the comparison of mean values of the flexural parameters of SECC samples prepared in laboratory and at the concrete batching plant. The plant specimens exhibited higher first-peak load ($P_1$) and peak load ($P_p$) than the laboratory specimens. The residual strength at deflections of L/600 and L/150 were also higher for the plant specimens. The toughness parameters, which is the area under the load-deflection curve up to L/150, $T_{150}^{D}$ for the plant specimens are approximately 97.4% and 90.3% of their corresponding laboratory samples' values. This indicates comparable flexural performance between the scale-up production and the laboratory production of the two SECC mixes.

Table 4: Flexural performance comparison between laboratory and scale-up production (plant)

| Test Items | Mean value of GGBS-ECC(plant) | Mean value of PFA-ECC(plant) | Mean value of GGBS-ECC(lab) | Mean value of PFA-ECC(lab) |
|---|---|---|---|---|
| $\boldsymbol{P_P}$, N | 27298.7 | 29545.8 | 26101.67 | 25852.41 |
| $\boldsymbol{f_P}$, MPa | 8.19 | 8.86 | 7.83 | 7.75 |
| $\boldsymbol{\delta_P}$, mm | 2.16 | 2.81 | 2.47 | 2.05 |
| $\boldsymbol{P_1}$, N | 22644.33 | 23919.40 | 20088.88 | 18674.02 |
| $\boldsymbol{f_1}$, MPa | 6.79 | 7.17 | 6.03 | 5.60 |
| $\boldsymbol{\delta_1}$, mm | 0.81 | 1.05 | 0.41 | 0.35 |
| $\boldsymbol{P_{600}^{D}}$, N | 18135.23 | 14326.47 | 21093.34 | 20369.27 |
| $\boldsymbol{f_{600}^{D}}$, MPa | 5.44 | 4.30 | 6.33 | 6.11 |
| $\boldsymbol{P_{150}^{D}}$,MPa | 26409.4 | 27273.6 | 22806.32 | 24993.12 |
| $\boldsymbol{f_{150}^{D}}$, N | 7.92 | 8.18 | 6.84 | 7.50 |
| $\boldsymbol{T_{150}^{D}}$, J | 40.8 | 38.35 | 41.90 | 42.45 |

Proceedings DOI: 10.21467/proceedings.8.2
ISBN: 978-81-688301-1-0

Series: AIJR Proceedings
ISSN: 2582-3922

For energy absorption capacity, the SECC samples were tested in accordance with BS EN 14488-5. A single portal frame with maximum load of 50 tons from Hangzhou POPWIL was used in this test. Test results, including load-deflection curves and energy absorption capacity-deflection curves , are shown in Figure 9 and Figure 10 below. The peak loads for PFA-ECC square panels ranged from 101.3 kN to 108.5 kN, while absorbed energy up to 25 mm deflection was 1722 J to 1904 J (1.7–1.9 times the EFNARC Class C/NGI Class E1000 value of 1000 J). For GGBS-ECC panels, peak loads were 96.9 kN to 99.2 kN, with absorbed energy of 1382–1786 J (1.4–1.8 times Class C).

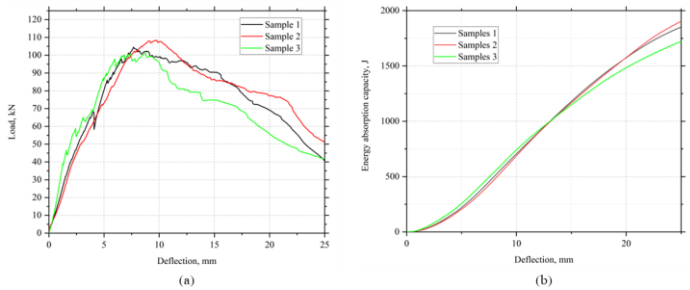



Figure 9: (a) Load versus deflection curves and (b) energy absorption capacity versus deflection curve for PFA-ECC

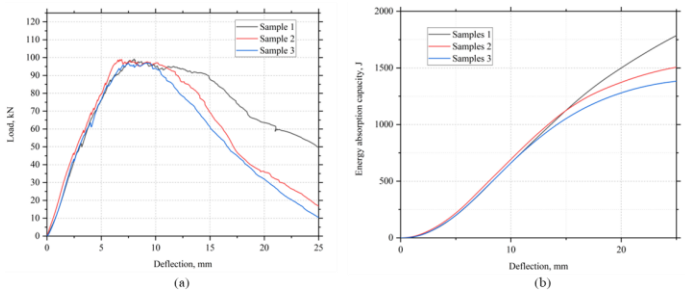



Figure 10: (a) Load versus deflection curves and (b) energy absorption capacity versus deflection curves for GGBS-ECC

Multiple cracks can be seen on all side-faces of the ECC square panels during and after the test (Figure 11(b)). There were no obvious cracks on the compressed surface, but several large cracks appeared on the backside, surrounded by numerous small radial cracks. However, these cracks did not penetrate through the specimen, and the specimen did not break into multiple pieces even after unloading, allowing the panels to withstand a certain load before loss of stability and retain load-bearing capacity.

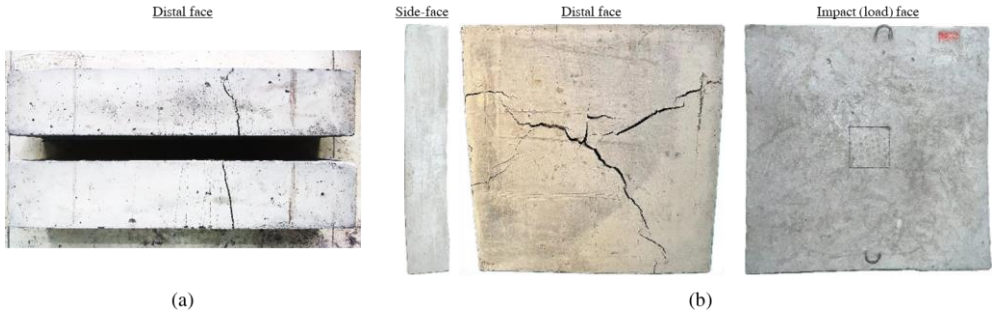



Figure 11: Multiple cracks in (a) flexure test specimens, and (b) panel test specimens in the scale-up production trial

As shown in Figure 12(a) below, test results indicate that plant-produced GGBS-ECC and PFA-ECC panels exhibited strong energy absorption, achieving EFNARC Class C/NGI Class E1000. Average energy absorption capacities were 1558 J for GGBS-ECC (plant) and 1825 J for PFA-ECC (plant), exceeding laboratory samples

by 17.7% and 26.8%, respectively. Overall, it shows that the scale-up production trial preserved the designed SECC mixes' performance with notable enhancement.

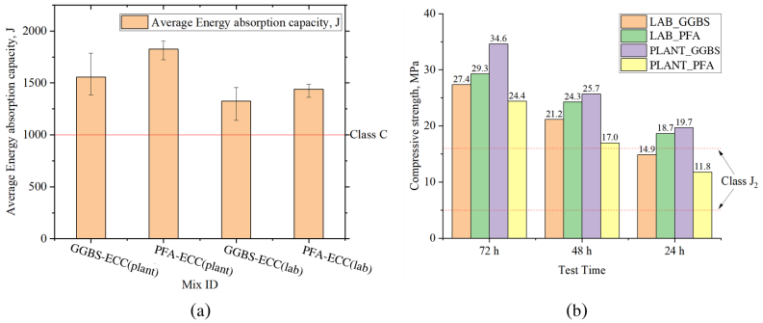



Figure 12: (a) Average energy absorption capacities, and (b) early-age compressive strength results

### *3.3 Early-age compressive strength*

Cube samples were tested at the ages of 1 day, 2 days and 3 days in accordance with BS EN 12390. A Shanghai SUNS YAW-2000 hydraulic testing machine was used for this test. Figure 12(b) above compares compression test results between laboratory and plant specimens. Plant GGBS-ECC specimens showed notably higher compressive strength than laboratory ones, while plant PFA-ECC specimens were slightly lower. Variations may have arisen from cube casting workmanship, mixing quality or related factors. Overall, all specimens met Class J2 requirements per BS EN 14487-1 based on 1-day compressive strength.

## 4 SITE SPRAY TRIAL

### *4.1 Site spray trial at the Joint Cavern Development project site*

Considering the foreseen shortage of PFA supply in Hong Kong, only one site spray trial was conducted for the GGBS-ECC mix inside the caverns of the Joint Cavern Development at the Anderson Road Quarry Site Project. Glorious Concrete Ltd (Glorious) supplied the required GGBS-ECC mixes for this trial. The concrete batching plant is located in Tuen Mun (Figure 13), with a production capacity of 3000 cubic metres per day.



Figure 13: Concrete batching plant of Glorious Concrete Ltd in Tuen Mun

The proportions of the GGBS-ECC mix used in this trial are summarised in Table 5. To refine the mix design suited to the use of local constituent materials supplied by Glorious, the transportation time (roughly 50 minutes) and the use of an accelerator (BASF SA167 in a mass ratio of 0.06 for fast-setting and expansion control) in the spraying machine were also considered, and an additional laboratory trial was conducted before scale-up production.

Table 5: Mix proportions of GGBS-ECC (mass ratio, PVA fibre vol. ratio 0.02) in a volume of 3 $m^3$

| ID | OPC | CSA | GGBS | Water | Sand | HPMC | SP |
|---|---|---|---|---|---|---|---|
| GGBS-ECC | 0.95 | 0.05 | 1.00 | 0.81 | 0.72 | 0.001 | 0.007 |

Proceedings DOI: 10.21467/proceedings.8.2
ISBN: 978-81-688301-1-0

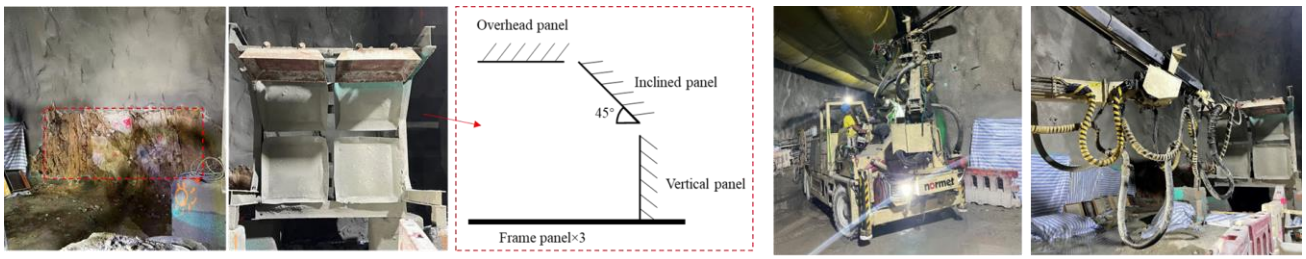
Series: AIJR Proceedings
ISSN: 2582-3922

### *4.2 Set-up of the site spray trial*

The site spray trial was designed primarily for testing sprayability and uniformity, as well as adhesiveness of the GGBS-ECC lining to rock substrates up to a certain design thickness (e.g., 10 cm, Table 5). A rock surface panel (representing a wall scenario) and a steel frame with a set of two vertical panels, a set of two inclined panels at 45 degrees to the horizontal and a set of two overhead panels (representing a tunnel crown scenario) were adopted to simulate a full tunnel/cavern setting as shown in Figure 14(a). In practice, the actual thickness varies with overall profile roughness and unevenness. The Normet Spraymec 8100 VC used in routine industrial operation was adopted for this trial, as shown in Figure 14(b).

Table 5: Dimensions of spraying test set-up

| Test Set-up | Panel Dimensions |
|---|---|
| Rock surface panel | 4500 × 1500 × 100 mm |
| Steel frame | 1200 × 1200 × 300 mm |




(a) (b)

Figure 14: (a) Spraying test setup with a rock surface panel and a steel frame and (b) Normet Spraymec 8100 VC

Other than the spraying test mentioned above, cube, prism and square panel samples were prepared for the routine quality production tests. All specimens were demoulded after 24 hours from casting in the site spray trial and transported to HKUST Concrete Laboratory for air curing. The required testing ages varied according to the specific test requirements as described in the subsequent sections. Finally, structural integrity was assessed through two-week deformation monitoring and field survey to see if the lining was affected by shrinkage and blast vibration caused by further construction work. Five monitoring points (MT1, MT2, MT3, MT4, and MT5) were installed on the rock panel surface and the adjacent portions of the cavern wall. Results suggested no observable deformation trend, with movement within 2 mm, indicating adequate structural integrity in this setting.

### *4.3 Verification of mechanical performance*

Mechanical performance of the GGBS-ECC mix in the site spray trial was evaluated through testing of compressive strength, flexural strength, energy absorption capacity and bond strength. Early-age compressive strength performance was verified through a penetration needle test (at 1 hour) and a stud-driving test (at 8 hours) on rock surface panels, in accordance with BS EN 14488-2. Conventional cube tests at ages beyond 8 hours according to CS1:2010 / BS EN 12390-3 were also performed for long-term strength verification. The satisfactory test results are shown in Table 6.

Table 6: Test results of compressive strength for GGBS-ECC samples

| Age of SECC | Compressive strength | | | |
|---|---|---|---|---|
| | Test values (MPa) | | | Mean value (MPa) |
| | Sample 1 | Sample 2 | Sample 3 | |
| 1h (Penetration needle) | 0.42 | 0.55 | 0.51 | 0.5* |
| 8h (Stud driving) | 2.80 | 2.30 | 2.50 | 2.5* |
| 1d | 12.50 | 13.40 | 14.70 | 13.5 |
| 7d | 37.30 | 41.20 | 40.70 | 39.7 |
| 28d | 48.00 | 50.10 | 46.80 | 48.3 |

* Both 1h and 8h compressive strength performance achieved Class J2 as per BS EN 14487-1.

According to BS EN 14487-1, the early-age compressive strength of the GGBS-ECC mix reached the $J_2$ strength class. The 28-day mean compressive strength of 48.3 MPa was similar to the laboratory and scale-up production trial results (45 MPa to 55 MPa). In particular, due to the strain-hardening of ECC, a grade strength is not specified in this study. The current strength performance may be viewed as similar to the standard strength performance of grade 40 concrete.

For flexural strength performance, prisms were sawn from the test panels and tested according to ASTM C1609 as discussed in Section 3. The flexural stress against central deflection curves of the ECC specimens at ages of 7 days and 28 days are shown in Figure 15 below. Calculated flexural parameters are summarised in Table 7.

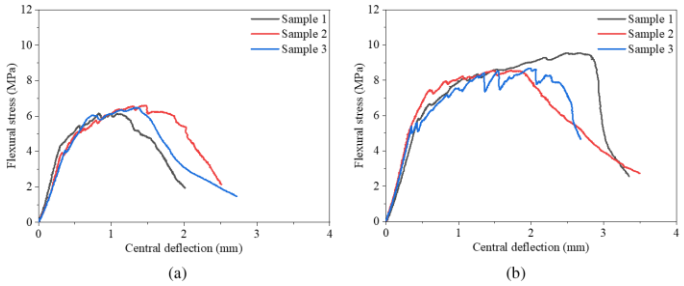



Figure 15: Flexural stress versus central deflection curve of (a) 7-day and (b) 28-day GGBS-ECC beams

The 7-day and 28-day mean first peak flexural strength values of the GGBS-ECC mix are 4.1 MPa and 6.2 MPa, respectively, while the 7-day and 28-day mean peak flexural strength values are 6.4 MPa and 9.0 MPa, respectively. Similar to the results of the scale-up production trial, multiple cracks can be observed on the 28-day GGBS-ECC beam specimen as shown in Figure 16(a). Overall, central deflection values ranged from 2 mm to 4 mm, which varied with sample compactness. Test results were satisfactory and comparable to the laboratory and scale-up production performance.

In addition to directly examining the flexural test results, Table 7 also shows the comparison with the minimum and maximum results according to a database from BS EN 14488-3 and ASTM C1609, composed of 26 sets of three or four replicate test specimens that were cast in laboratory and tested by one operator using a closed-loop, servo-controlled hydraulic universal-testing machine. Except for the deflection, which was slightly smaller than the maximum value, all other test results demonstrated close resemblance to or better performance than the maximum values in the said database.

Table 7: Flexural parameters of ECC samples and test results from a database

| Test Items | Mean value of GGBS-ECC (7d) | Mean value of GGBS-ECC (28d) | From the database of BS EN 14488-3 and ASTM C1609 | |
|---|---|---|---|---|
| | | | Minimum value | Maximum value |
| $P_P$, N | 21366.3 | 29759.7 | 9869 | 27071 |
| $f_P$, MPa | 6.4 | 9.0 | 2.44 | 7.46 |
| $\delta_P$, mm | 1.3 | 2.1 | 0.03 | 2.44 |
| $P_1$, N | 13749.6 | 20787.9 | 9868 | 27071 |
| $f_1$, MPa | 4.1 | 6.2 | 2.44 | 7.12 |
| $\delta_1$, mm | 0.4 | 0.5 | 0.03 | 0.06 |
| $P^D_{600}$, N | 16157.1 | 20572.7 | 4828 | 24076 |
| $f^D_{600}$, MPa | 4.9 | 6.2 | 1.20 | 7.00 |
| $P^D_{150}$,MPa | 13884.2 | 28374.1 | 5193 | 18588 |
| $f^D_{150}$,N | 4.2 | 8.5 | 1.29 | 5.41 |
| $T^D_{150}$, J | 32.0 | 45.2 | 10 | 42 |

Proceedings DOI: 10.21467/proceedings.8.2
ISBN: 978-81-688301-1-0

Series: AIJR Proceedings
ISSN: 2582-3922




Figure 16: Multiple cracks in (a) flexure test specimens and (b) square panel test specimens for GGBS-ECC

For energy absorption capacity, square panel specimens were tested in accordance with BS EN 14488-5. The load-deflection curves and the energy absorption capacity-deflection curves are shown in Figure 17(a) and Figure 17(b), respectively. Table 8 summarises the peak loads and energy absorption capacities. Thickness correction was performed as the on-site sprayed panels measured approximately 100 mm at the edges with a slight rise to around 120 mm toward centre. As shown in Figure 16(b) above, the test panel typically failed with a formation of cross cracks. Overall, test results achieved EFNARC Class C/NGI Class E1000 (1000 J), which was satisfactory and comparable to the scale-up production performance.

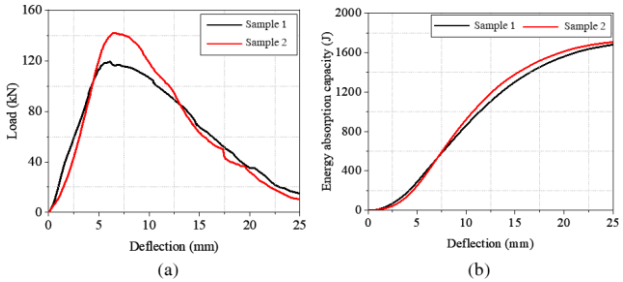



Figure 17: (a) Load versus deflection curves and (b) energy absorption capacity versus deflection curves for GGBS-ECC

Table 8: Summary of energy absorption capacities

| Mix ID | Sample ID | Peak Load (kN) | Energy absorption capacity | |
|---|---|---|---|---|
| | | | Test value (J) | Corrected value (J) |
| GGBS-ECC | 1 | 119.1 | 1680.0 | 1104.6 (t = 115 mm) |
| | 2 | 142.0 | 1706.5 | 1038.6 (t = 118mm) |

Finally, in-situ bond performance was assessed through in-situ coring for further laboratory pull-off / Brazilian test. While a few attempts were made, the coring results showed failure either within the cracked rock substrate or at the glue between the dolly and the GGBS-ECC surface. These results suggested that the bond strength between GGBS-ECC and rock may well exceed the adhesion of the testing glue. Given consistent outcomes from the attempts and further field observations, the spraying process appeared to have no adverse impact on bond strength performance. It should be noted that, however, bond strength performance is more sensitive to spraying technique and workmanship as well as preparation of the rock substrate surface beforehand.

### *4.4 Spraying performance and final appearance of applied GGBS-ECC*

Figure 18 shows the spraying process and the final appearance of GGBS-ECC applied to the rock surface panel. Despite the demonstrated minimal rebound and satisfactory mechanical performance, the applied GGBS-ECC surface appeared nodular and irregular, with some localised cavities. These imperfections are likely attributable to concentrated spraying over a limited area, the long (approximately 1 hour) interval between plant mixing and on-site application, and the lack of calibrated spraying parameters and operator technique specific to ECC. Refinement of the mix design together with improved spraying procedures and crew training will be required to achieve a smoother and more uniform finish.



(a) (b)

Figure 18: (a) Spraying of steel frame panels and (b) final appearance of GGBS-ECC applied to the rock surface panel

## 5 CONCLUSIONS AND WAY FORWARD

This study developed two feasible SECC mixes using locally available materials, with the GGBS-ECC mix selected for the site spraying trial. Mechanical tests confirmed the characteristic strain-hardening behaviour under flexure, high energy absorption capacity, and consistent quality across laboratory, plant, and field conditions. Certain aspects warrant further investigation, including self-healing and self-stressing in the field, surface texture refinement through adjustments to mix & spraying, and crew training (e.g. nozzlemen). This work provides fresh insights into SECC for tunnel lining applications in Hong Kong. Leveraging its self-healing, self-stressing, high ductility, and residual mechanical properties, SECC offers significant potential to enhance water tightness, reduce maintenance costs, and enable more cost-effective design solutions in tunnelling applications. Wider adoption will require streamlined ECC production logistics and a progressive refinement of structural design methodologies to fully capture ECC's potential.

## ACKNOWLEDGEMENTS

The authors gratefully acknowledge the collaboration of the Joint Cavern Development at Anderson Road Quarry Site project team in facilitating the site spraying trial, as well as the support of the two ready-mix suppliers in producing the materials. This paper is published with the permission of the Head of the Geotechnical Engineering Office and the Director of Civil Engineering and Development, the Government of the Hong Kong Special Administrative Region.

## PUBLISHER'S NOTE

AIJR remains neutral with regard to jurisdictional claims in published maps & institutional affiliations.

## REFERENCES

Ding, Z., Wen, J., Li, X., Fu, J. & Ji, X. 2020. Mechanical behaviour of polyvinyl alcohol-engineered cementitious composites (PVA-ECC) tunnel linings subjected to vertical load. Tunnelling and Underground Space Technology, 95: 103151.

Ghosh, S.K. 2009. Self-Healing Materials: Fundamentals, Design Strategies, and Applications. Wiley-VCH.

Khandelwal, M. & Singh, T.N. 2009. Prediction of blast-induced ground vibration using artificial neural network. International Journal of Rock Mechanics and Mining Sciences, 46: 1214–1222.

Li, V.C. 1993. From micromechanics to structural engineering — the design of cementitious composites for civil engineering applications. Doboku Gakkai Ronbunshu, 1993(471): 1–12.

Li, V.C. 2019. Engineered cementitious composites (ECC): bendable concrete for sustainable and resilient infrastructure. Springer.

Li, V.C. 2003. On engineered cementitious composites (ECC). A review of the material and its applications. Journal of Advanced Concrete Technology, 1: 215–230.

Li, V.C. & Leung, C.K.Y. 1992. Steady-state and multiple cracking of short random fiber composites. Journal of Engineering Mechanics, 118(11): 2246–2264.

Qian, C., Zhao, Y.C., Sun, M.G., Chen, J.X., Luo, Y.B. & Li, Z. 2025. Study on safety distance of pedestrian cross passages in single-tube four-lane highway tunnels. Chang'an Daxue Xuebao (Ziran Kexue Ban)/Journal of Chang'an University (Natural Science Edition), 45(5): 81–91.

Van Tittelboom, K. & De Belie, N. 2013. Self-Healing in Cementitious Materials—A Review. Materials, 6(6): 2182–2217.

Yang, Y., E.H. Yang, and V.C. Li 2011. Autogenous Healing of Engineered Cementitious Composites at Early Age. Cement and Concrete Research, 41(2), 176-183.

Zhu, H., Zhang, D., Wang, Y., Wang, T. & Li, V.C. 2021. Development of self-stressing Engineered Cementitious Composites (ECC). Cement and Concrete Composites, 118: 103936.